NeuroImage 251 (2022) 119002

Contents lists available at ScienceDirect

NeuroImage

journal homepage: www.elsevier.com/locate/neuroimage

An interdisciplinary computational model for predicting traumatic brain injury: Linking biomechanics and functional neural networks

Taotao Wu[a], Jared A Rifkin[a], Adam Rayfield[a], Matthew B. Panzer[b,c], David F. Meaney[a,d,*]

[a] Department of Bioengineering, University of Pennsylvania, 240 Skirkanich Hall, 210 S 33rd St, Philadelphia, PA 19104, United States
[b] Department of Mechanical and Aerospace Engineering, University of Virginia, Charlottesville, VA, United States
[c] Department of Biomedical Engineering, University of Virginia, Charlottesville, VA, United States
[d] Department of Neurosurgery, University of Pennsylvania, Philadelphia, PA, United States

ARTICLE INFO

Keywords:
Kuramoto model
Balloon-Windkessel model
Functional connectivity
Structural connectivity
Concussion

ABSTRACT

The brain is a complex network consisting of neuron cell bodies in the gray matter and their axonal projections, forming the white matter tracts. These neurons are supported by an equally complex vascular network as well as glial cells. Traumatic brain injury (TBI) can lead to the disruption of the structural and functional brain networks due to disruption of both neuronal cell bodies in the gray matter as well as their projections and supporting cells. To explore how an impact can alter the function of brain networks, we integrated a finite element (FE) brain mechanics model with linked models of brain dynamics (Kuramoto oscillator) and vascular perfusion (Balloon-Windkessel) in this study. We used empirical resting-state functional magnetic resonance imaging (MRI) data to optimize the fit of our brain dynamics and perfusion models to clinical data. Results from the FE model were used to mimic injury in these optimized brain dynamics models: injury to the nodes (gray matter) led to a decrease in the nodal oscillation frequency, while damage to the edges (axonal connections/white matter) progressively decreased coupling among connected nodes. A total of 53 cases, including 33 non-injurious and 20 concussive head impacts experienced by professional American football players were simulated using this integrated model. We examined the correlation of injury outcomes with global measures of structural connectivity, neural dynamics, and functional connectivity of the brain networks when using different lesion methods. Results show that injurious head impacts cause significant alterations in global network topology regardless of lesion methods. Changes between the disrupted and healthy functional connectivity (measured by Pearson correlation) consistently correlated well with injury outcomes ($AUC \geq 0.75$), although the predictive performance is not significantly different ($p > 0.05$) to that of traditional kinematic measures (angular acceleration). Intriguingly, our lesion model for gray matter damage predicted increases in global efficiency and clustering coefficient with increases in injury risk, while disrupting axonal connections led to lower network efficiency and clustering. When both injury mechanisms were combined into a single injury prediction model, the injury prediction performance depended on the thresholds used to determine neurodegeneration and mechanical tolerance for axonal injury. Together, these results point towards complex effects of mechanical trauma to the brain and provide a new framework for understanding brain injury at a causal mechanistic level and developing more effective diagnostic methods and therapeutic interventions.

1. Introduction

Traumatic brain injury (TBI) poses a rising challenge to public health. In 2014 alone, there were approximately 2.87 million TBI-related emergency department visits, hospitalizations, and deaths in the United States (Peterson et al., 2019). Despite the increased awareness of TBI among the general public and improved diagnostic classification, management, and prognosis of TBI, the underlying pathophysiology for TBI is not fully understood. A prevailing view is that the complex neurocognitive and neuropsychological deficits experienced by TBI survivors, many of whom do not have a focal brain injury detected by neuroimaging or histopathological analysis, are not explained by damage restricted to a single brain area. Rather, the diffuse distribution of the impact force leads to damage in several areas of the brain simultaneously. Given that cognitive functions of the brain depend on the coherent activity of complex brain networks (Fries, 2005), there is

* Corresponding author at: Department of Bioengineering, University of Pennsylvania, 240 Skirkanich Hall, 210 S 33rd St, Philadelphia, PA 19104, United States.
E-mail addresses: taotaowu@seas.upenn.edu (T. Wu), jarifkin@seas.upenn.edu (J.A. Rifkin), adamra@seas.upenn.edu (A. Rayfield), panzer@virginia.edu (M.B. Panzer), dmeaney@seas.upenn.edu (D.F. Meaney).

https://doi.org/10.1016/j.neuroimage.2022.119002.
Received 12 June 2021; Received in revised form 19 January 2022; Accepted 12 February 2022
Available online 14 February 2022.

increasing interest in using connectivity-based methods to understand how the diffuse patterns of damage throughout the brain interacts with the brain's inherent interconnectivity to cause the deficits following TBI. To this end, a series of studies measure the temporal dependence between regional activities recorded by neuroimaging techniques such as functional magnetic resonance imaging (fMRI), electroencephalography (EEG) or magnetoencephalography (MEG) to infer changes in the brain connectivity after TBI (Aerts et al., 2016).

Several empirical studies utilized the network approach to evaluate changes in brain networks following TBI. For example, growing evidence suggests that TBI may cause changes in (resting-state) functional connectivity (Churchill et al., 2018; Meier et al., 2017; Plourde et al., 2020; Virji-Babul et al., 2014). Although brain networks of injured and healthy groups showed no statistically significant differences in the global metrics (e.g., global efficiency, modularity, clustering coefficient), significant differences occurred in local network metrics (Virji-Babul et al., 2014). Similarly, both increased and decreased functional connectivity within local functional brain networks were found during the whole-brain analysis of resting-state fMRI (Churchill et al., 2018; Meier et al., 2017). For example, functional connectivity of the anterior default mode network (DMN) (Plourde et al., 2020) and a network of frontal, temporal, and insular regions (Churchill et al., 2018) was negatively correlated with symptom severity; the functional connectivity of a network with anti-correlated elements of the DMN and sensorimotor system (Churchill et al., 2018) was positively correlated with symptom severity. These results suggest a link between TBI, local functional networks, and post-injury symptoms. However, these findings were obtained from relatively small sample sizes with a cross-sectional design. It is, therefore, unknown how the brain function of the injured subjects compared to pre-injury brain function.

In parallel with these emerging clinical insights, computational neuroscience provides cellular- and systems-scale tools to shed light on understanding the alterations of physiology and cognitive abilities after brain injury. At the systems level, the impact of lesioning structural connectomes in neural dynamics (Váša et al., 2015) and resting-state functional connectivity (Cabral et al., 2012) show that TBI can cause significant disruptions to brain information processing. The removal of nodes from the network with specific network characteristics (e.g., nodes with high eigenvector centrality; hub nodes) decrease network synchrony while increasing metastability (Váša et al., 2015). Alternatively deleting and weakening edges (coupling strengths or connectivity) create functional networks with higher efficiency but less clustering, among other changes (Cabral et al., 2012).

These prior studies which systematically pruning an intact network clearly show the effect of removing nodes with particular characteristics, whether it was nodes that were most connected to other nodes, or nodes that represented critical pathways among smaller subnetworks within the brain. However, neurological diseases and disorders rarely follow such a systematic pruning process from the most connected to least connected node, or any other "ordered deconstruction" process. This is especially true of mechanical impact to the brain, which is complicated even more because the impact conditions experienced by one person is different from another. Indeed, we observed the regions most important for network information flow do not generally align well with brain regions that deformed the most during the impacts (Anderson et al., 2020). However, it is unknown how the expected structural damage to the brain from an impact could affect its functional state - e.g., would a concussive impact more likely cause a change in the synchrony of the brain compared to an impact that does not cause concussion? To answer this question more completely, one would need to incorporate methods to translate an impact to a change in the wiring of the brain, and then convert this change in wiring into an estimate of the functional brain network properties that occur after impact.

Computational models in biomechanics provide one part of this solution by accurately estimating the local mechanical response of brain tissue for a given external load. After mapping these models to the brain structures, finite element (FE) models provide an accurate representation of the macroscale brain anatomy (Giudice et al., 2019) and mesoscopic white matter tractography (Garimella and Kraft, 2017; Wu et al., 2019b) to provide a realistic prediction of intracranial brain motion for any given external head kinematics. These models are necessarily validated with experimental tests (Alshareef et al., 2020; Hardy et al., 2007), and undergo constant refinement to adjust for changes in the size of the brain, the physical characteristics of brain tissue, and the mode of traumatic loading (e.g., impact versus blast overpressure exposure). From these biomechanical models, numerous kinematics-based metrics (Gabler et al., 2018, 2019) and tissue-level strain metrics (Giordano and Kleiven, 2014; Hajiaghamemar et al., 2020; Sahoo et al., 2016; Wu et al., 2021b) emerged from the simulation of real-world or laboratory impacts to more accurately predict the impact scenarios that are likely to cause brain injury, and other impacts which could be considered safe. Until now, these biomechanical models are based on the premise that brain regions are more likely to experience larger deformation during an injurious impact and the brain injury risk is solely from the severity and extent of this impact-based damage. Existing approaches provide no inference on how brain deformations affect the global function of the brain network. Recent efforts to integrate brain mechanics to network analysis provide encouraging insights into the underlying basis of cognitive impairments after TBI (Anderson et al., 2020; Kraft et al., 2012; Wu et al., 2019a), but the variety of these techniques face significant challenges in merging the mechanical response and brain functional response, both are vital steps to fully understand the mechanism of TBI (Meaney et al., 2014).

In this study, we combined a FE brain model, a neurodynamic model, and a hemodynamic model derived from neural dynamics to explore how an impact can affect the global function of brain networks. We first tuned the neurodynamic model to simulate empirical resting-state functional connectivity of a healthy brain. Once calibrated for a healthy subject, we utilized the FE model to simulate 53 head impacts experienced by professional American football players (Sanchez et al., 2019) with known head kinematics and injury outcomes (no concussion, concussion). Based on the results of FE simulations, lesions to the structural brain network were implemented to assess the change in the regional brain perfusion from the hemodynamic model. Together, combining the lesioned neurodynamic model and hemodynamic model provided estimates of the brain functional connectivity after simulated impact. We examined the correlation of injury outcomes with global measures of structural connectivity, neural dynamics, and functional connectivity of the brain networks. Our main hypothesis was that including measures in the changes of brain network structural and functional properties after impact would improve TBI prediction. Our findings show that simulated injury to brain network dynamics produces complex changes in synchrony and network structure, mirroring changes observed in patients after TBI. Moreover, this approach highlights differences that can emerge in brain dynamics when injury patterns are changed. Together, this approach provides an entry point for understanding brain injury at a causal mechanistic level.

2. Methods

2.1. Simulation of healthy subjects

2.1.1. Neuroimaging data and preprocessing

Publicly accessible, high-quality neuroimaging and cognitive data from the healthy participants of the human connectome project (HCP) were used in this study. Diffusion MRI data were reconstructed in DSI Studio (http://dsi-studio.labsolver.org) using q-space diffeomorphic reconstruction (QSDR) (Yeh and Tseng, 2011) with a mean diffusion distance ratio of 1.25. Deterministic whole-brain fiber tracking was performed with an angular cutoff of 55, step size of 1.0 mm, the minimum length of 10 mm, spin density function smoothing of 0.0, the maximum

length of 400 mm until 1000,000 streamlines were reconstructed for each subject.

A cortical parcellation atlas (Schaefer et al., 2018), based on resting-state functional magnetic resonance imaging (rs-fMRI), was used to "filter in" the tracks that pass through the regions (100 regions clustered into seven networks) to generate a weighted structural connectivity (SC) matrix (100 × 100) and a distance matrix (100 × 100). Each network edge in the connectivity matrix corresponds to the number of streamlines that interconnect two regions normalized by the total number of streamlines, and each network edge in the distance matrix is the inter-regional mean fiber length. A generic structural network (ID:108,020, male) was selected to represent the population because its SC matrix was closest to the average SC matrix ($n = 1065$). The preprocessed empirical rs-fMRI (Glasser et al., 2013) from the corresponding HCP subject were also parcellated using Schaefer's atlas. Pearson correlation coefficients were calculated between each pair of ROIs to generate the functional connectivity (FC) matrix. One FC matrix was generated by taking the average of the FC matrices obtained using rs-MRI data acquired in 2 phase encoding directions (rfMRI_REST1_RL, rfMRI_REST1_LR).

2.1.2. Kuramoto model and hemodynamic model

The resting-state cortical neural dynamical activity was simulated using the Kuramoto oscillators model with time delays (Kuramoto, 1984; Yeung and Strogatz, 1999), in which each oscillator was assigned to a cortical node (or ROI) and connected based on coupling strengths and fiber lengths of brain structural connectivity. The synchronization behavior of a system of coupled oscillators ($N = 100$) in the Kuramoto model obeys the following delay differential equations:

$$\dot{\theta}_i = \omega_i + K\sum_{j=1}^{N} C_{ij} sin\left(\theta_j\left(t-\tau * D_{ij}\right) - \theta_i(t)\right),\ i = 1, \ldots, N$$

Where θ_i and ω_i denotes the phase and intrinsic frequency of node i. Phases were initialized randomly with uniform distribution between 0 and 2π. Natural frequencies were uniformly distributed around a 60 Hz mean with a 1 Hz standard deviation to simulate fast oscillatory activity in the gamma frequency band (Cabral et al., 2012). K is the global coupling strength, and C_{ij} is the relative coupling strength between nodes i and $j$computed from the structural connectivity matrix. C_{ij} was normalized such that the average of all non-zero edge weights equaled 1. The mean time delay (τ) and the individual time delay between nodes i and j was assumed to be proportional to D_{ij}, which was calculated by normalizing the distance matrix by the mean fiber length. Model parameters K and τ were tuned with respect to empirical rs-fMRI data (Fig. 1). The time delays ($\tau * D_{ij}$) were rounded at 2 ms resolution to expedite the most time-consuming process of the simulation while preserving accuracy. The delay differential equations were numerically solved using the extended Runge–Kutta method (Shampine and Thompson, 2001) implemented in MATLAB (dde23.m, The MathWorks Inc., Natick, MA).

The sine of the phases ($sin\ (\theta_i)$) generated by the Kuramoto model were transformed into simulated blood-oxygen-level-dependent (BOLD) signals (y) using the Balloon–Windkessel hemodynamic model (Friston et al., 2000), as detailed in the following equations:

$$r_n(t) = sin\left(\theta_n(t)\right)$$

$$\frac{\tau_0 \partial v_n(t)}{\partial t} = f_n - v_n^{\frac{1}{\alpha}}$$

$$\frac{\partial f_n(t)}{\partial t} = s_n$$

$$\frac{\partial s_n(t)}{\partial t} = r_n - \kappa_s s_n - \gamma_f\left(f_n - 1\right)$$

$$\frac{\tau_0 \partial q_n(t)}{\partial t} = \frac{f_n\left(1-\left(1-E_0\right)^{\frac{1}{f_n}}\right)}{E_0} - \frac{v_n^{\frac{1}{\alpha}} q_n}{v_n}$$

Table 1
Parameters of Balloon-Windkessel hemodynamic model.

Parameters	Description	Value
α	Grubb's exponent	0.32
κ_s	Rate of signal decay	0.65 (1/s)
γ_f	Rate of flow-dependent elimination	0.41 (1/s)
τ_0	Hemodynamic transit time	0.98 (s)
E_0	The resting oxygen extraction fraction	0.34
V_0	Resting blood volume fraction	0.02

$$y(t) = V_0\left(k_1\left(1-q_n\right) + k_2\left(1-\frac{q_n}{v_n}\right) + k_3\left(1-v_n\right)\right)$$

$$k_1 = 7E_0$$

$$k_2 = 2$$

$$k_3 = 2E_0 - 0.2$$

The model parameters and corresponding parameters settings are shown in Table 1. The differential equations were numerically solved using the explicit Runge-Kutta method implemented in MATLAB (ode45.m, The MathWorks Inc., Natick, MA). Simulations were run for 200 s, with the first 20 s discarded to remove transient effects. We down-sampled the simulated BOLD signals at a time-step of 0.72 s to achieve the same resolution as the empirical data and then calculated the simulated FC matrix based on pairwise Pearson correlation.

We defined a bounded domain to tune the model parameters K and τ for a healthy subject. To simplify further computation, we restricted the coupling strength to 0–20 and the mean delay time to a biologically plausible 0–10 ms in the range of physiologically realistic values for white matter tracts (Waxman, 2006). The cost function was defined as the absolute difference between the mean strength of the simulated and empirical FCs. Since negative values might reflect anti-correlated dependencies, the absolute values were used when calculating the mean strength. The optimization was performed using a manual search to find the location of the minimum cost function on the bounded parameter space with a termination criterion of 1% absolute error. Initially, we conducted an automatic optimization using the matlab fmincon function for the subject (ID:103,007) provided in the supplementary material, but it was a very time-consuming process given that each simulation takes about 20 h on our computers. Both the manual search and automatic search found the optimal location in a similar metastable regime, so a manual search was performed on the final representative subject to the error limit (1%) specified.

2.2. Simulation of functional network following head impact

Following model tuning for the resting-state functional connectivity of the healthy subject, we investigated the correlation between network measures and injury outcomes by simulating the head impact in professional American football games. An overview of the study workflow is shown in Fig. 2; each step of this process is explained in detail in the following sections.

2.3. Finite element simulations and injury data

The football impacts are helmet-to-helmet hits videotaped in professional American football games between 1996 and 2001 and experimentally reconstructed using anthropomorphic test dummies in a testing laboratory (Pellman et al., 2003; Sanchez et al., 2019). Apart from the head kinematics and injury outcomes, individual brain anatomical features and connectivities are not available. The concussion cases were independently verified by two team physicians who reviewed the

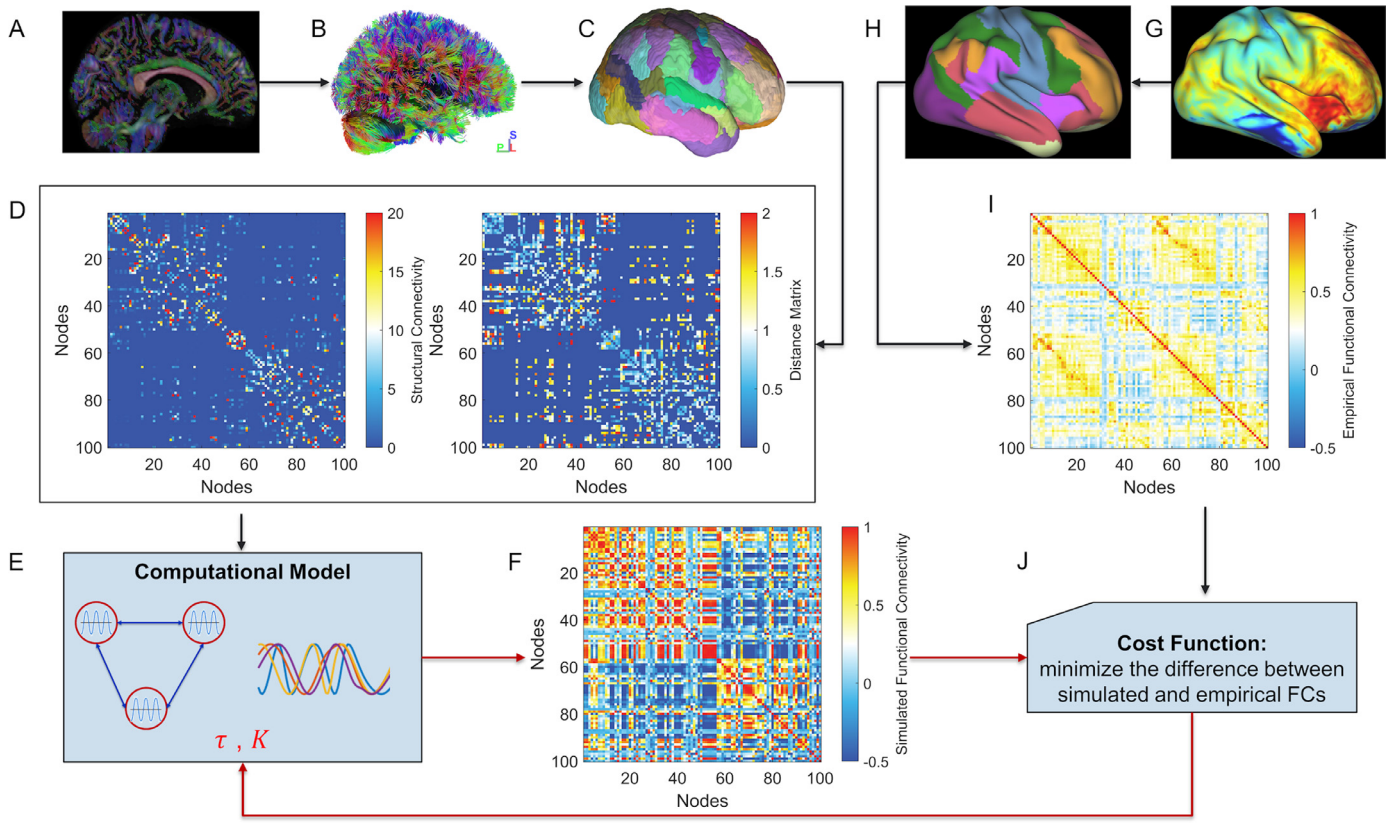

Fig. 1. Summary of model tuning methods. (A) Diffusion MRI of the generic subject was used to reconstruct fiber tractography (B); The cortical regions were organized first into 100 areas (parcellations), which were then consolidated into seven networks atlas in MNI space (C); (D) The structural connectome (D) was used to build a Kuramoto oscillator model (E), the results of which were used in a Balloon–Windkessel hemodynamic model to estimate perfusion in each nodal area. A functional connectivity (F) was derived from the estimate of perfusion. The estimate of FC was compared to the measured resting state functional connectivity measured directly in the subject (I); (H) Schaefer's 100 parcels seven networks atlas in fsLR32k space; (I) Empirical FC of the generic subject; (J) Cost function to minimize the difference between the simulated and empirical FCs provided an estimate of the model parameters which optimized the match between predicted and measured FC.

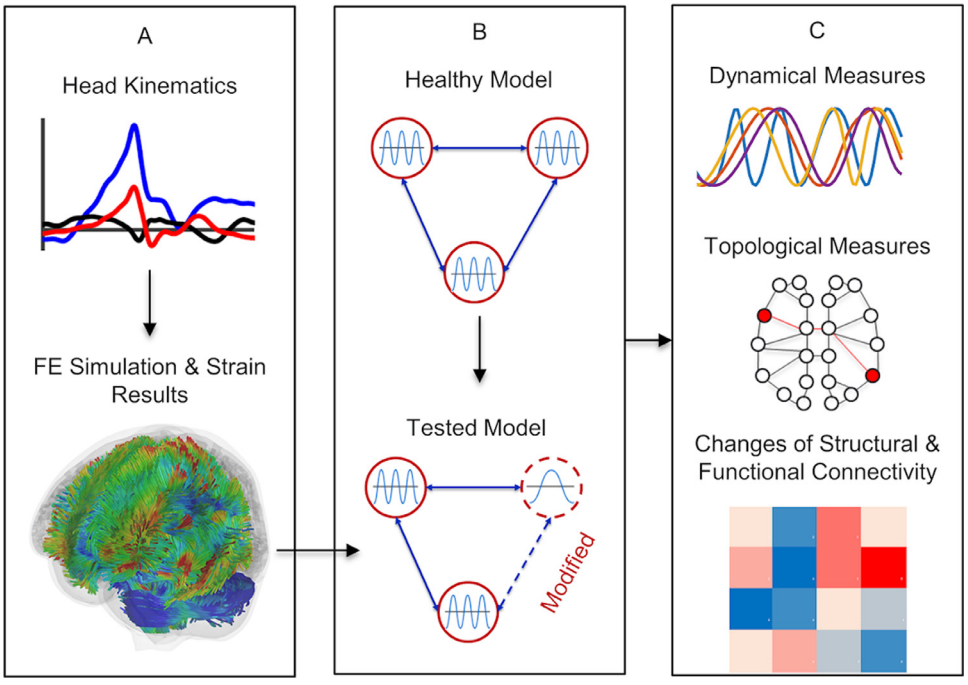

Fig. 2. Summary of injury study. (A) Finite element simulations of the football head impact provided an estimate of how nodes and edges in the brain network would be damaged after an impact; (B) Computational models used these estimates of how the nodes and edges within the network were affected by the impact to predict resting-state brain networks after head impacts; (C) Using both measures from the neural dynamics and subsequent functional connectivity, we assessed the utility of several neural network measures for predicting injury.

clinical information based on the definition of concussion used by the American Congress of Rehabilitation Medicine at that time (this definition is provided in the supplementary material). Of the verified concussion cases, most players exhibited multiple symptoms; memory problems, cranial nerve symptoms, headaches, abnormal immediate recall, dizziness, and nonspecific cognition problems/complaints were the most common symptoms and complaints.

A three-dimensional finite element human brain model with white matter axonal tracts explicitly modeled was utilized to simulate the reconstructed professional football impacts. The brain FE model to represent a 50th percentile male was previously validated for brain deformation under various loading conditions and showed good biofidelity (Alshareef et al., 2021; Wu et al., 2019b). The embedded axonal tracts were extracted from the population-averaged tractography template (HCP-842) of the human connectome project (Yeh et al., 2018). A total of 53 valid cases, including 33 non-injurious and 20 concussive head impacts, were simulated by prescribing the six-degrees-of-freedom experimental linear and rotational head kinematics to the FE brain model through the center of gravity of the head. All FE simulations were solved using LS-DYNA (v971 R9.2.0, double precision; LSTC, Livermore, CA).

2.4. Lesion methods: linking strain to the disruption of neural network

Traumatic brain injury is considered a mixture of focal and diffuse injury throughout the brain. The pathological consequences include neuronal injury, damage to the supporting vascular network, and disruption of the connections that exist across the brain architecture. From a network perspective, the cognitive deficits induced by TBI would be a result of lesions to the nodes or the edges from the neural network perspective. To this end, two methods were used to correlate strain results from the above FE simulations to alterations in brain networks or the neurodynamic model.

Our first method linked the local deformation to a decline in neural activity within individual brain regions. This model was based on the combined observations that (1) FE model-predicted tissue strain positively correlates with the percentage of the neuronal loss observed *in vivo* (Mao et al., 2010), and (2) both neuronal firing rate and oscillation frequency decreases as either neurodegeneration or neuronal inactivation increases (Gabrieli et al., 2020). Mild traumatic brain injury does not lead to widespread neuronal degeneration, but it does cause disruption in the synchronization of networks *in vitro* and a broad reduction in activation of neural circuitry *in vivo* (Hansen et al., 2018; Nguyen et al., 2021; Rogers and Gross, 2019), presumably from the temporary inability of some neurons to fire action potentials in the network (Mott et al., 2021). From a modeling standpoint, this phenomenon can be modeled by reducing the natural oscillator frequencies in nodes of the Kuramoto model in direct proportion to the peak deformation occurring within the brain region represented by the node (Fig. 3, node-based method). In this study, we use the cumulative strain damage measure (CSDM) to estimate the effect of an impact on the oscillation frequency of nodes in the neural network. The brain FE model was segmented into 100 regions of interest (ROI) according to the Schaefer parcellation atlas after matching the anatomy using a morphing technique (Wu et al., 2019b, Fig. 3A–C). For each ROI and impact condition, the fraction of the region experiencing strain levels higher than a critical threshold of 15% (CSDM15) or 25% (CSDM25) was calculated (Fig. 3E). Based on the correlation between strain, neurodegeneration level, and frequency (Fig. 3F), we modified the oscillation frequency for each node in the Kuramoto model (Fig. 3G) for each impact.

The second lesion method relates lesions to white matter tracts to the reduction of SC edge strength using the parcellated mesh, the path of white matter tracts connecting different regions, and the predicted axonal strain along these tracts (Fig. 4A–D, termed edge-based method). The mechanical tolerance for axonal injury was expressed as a risk function (statistical modeling of the occurrence of injury) of the axonal Lagrangian strain, determined by comparing morphological injury and electrophysiological impairment to *in vivo* tissue strain produced by dynamically stretching the optic nerve of an adult male guinea pig (Bain and Meaney, 2000). When applying the edge-based method for a given head impact, the axonal deformation in the FE brain was mapped to nodes of the network based on the parcellation atlas. The 100 ROIs were also used to segment the explicit tracts in the FE brain, the maximum tensile strain of the axonal tracts connecting each pair of ROIs was computed, resulting in a maximum axonal strain (MAS) matrix (100×100) quantifying the brain deformation for a given impact case (Fig. 4D, E). Based on the risk function of axonal damage with respect to axonal strain (Fig. 4F), the modified structural connectome (Fig. 4G) after a certain impact can be modified based on the strain metric in each edge.

2.5. Potential injury metrics

In this study, a variety of potential injury metrics were evaluated for their correlation with brain injury. Depending on their underlying information, these metrics belong to the five categories: measures describing head motion, tissue deformation, neural dynamics, structural networks, and functional networks. Head kinematic measures include peak resultant angular velocity (ω_{max}) and peak resultant angular acceleration (α_{max}); tissue deformation metrics include the 95th percentile maximum principal strain (MPS95) and CSDM25, these metrics have previously shown good correlation with injury outcomes for this dataset (Anderson et al., 2020).

Neural dynamical measures were evaluated as potential injury metrics. In the Kuramoto model, network dynamics were characterized by the mean and the standard deviation of the amplitude of the instantaneous synchrony $R(t)$ over time. We considered the mean $R(t)$ and an index of global synchrony and the standard deviation of $R(t)$ as an index of metastability. $R(t)$ is defined by:

$$R(t)e^{i\theta(t)} = \frac{1}{N}\sum_{n=1}^{N} e^{i\theta_n(t)}$$

Common topological measures of the tested brain networks (including modified SC and simulated FC) were also evaluated for their correlation with the injury. These most used topological metrics were characteristic path length (CPL) (Watts and Strogatz, 1998), global efficiency (GE) (Latora and Marchiori, 2001), local efficiency (LE) (Wang et al., 2017), clustering coefficient (CC) (Watts and Strogatz, 1998) and modularity (M) (Newman, 2006). A brief description of each metric is provided in the supplementary material (Section A2, Table A1). These methods were initially developed to describe the topology of networks with unweighted (binary), undirected, and positive weight links. To compute distance-based graph metrics (e.g., the characteristic path length or the global-efficiency) from weighted brain graphs, the link weights were substituted with their reciprocal (Rubinov and Sporns, 2010). For correlation-based FC, self-connections were deleted, and negative weights were set to zero (Rubinov and Sporns, 2010). Topological metrics were evaluated using the Brain Connectivity Toolbox (Rubinov and Sporns, 2010).

To quantify the differences between simulated FC of healthy subjects and tested subjects, the FC matrices were unrolled into vectors and the Pearson correlation (PC) between the vectors themselves was computed. Geodesic distance (GD) (Venkatesh et al., 2020) was also used to compare SC and FC matrices, given that SC and FC are positive semidefinite matrices.

2.6. Simulation using random parcellation and random network

Until now, our simulations focused on testing the correlation between changes in network dynamics and the likelihood of injury. To test the strength of this approach, we repeated the same analysis above using *random* parcellation and *random* network wiring. In contrast to the Schaffer 100 parcellation approach, we generated spatially random

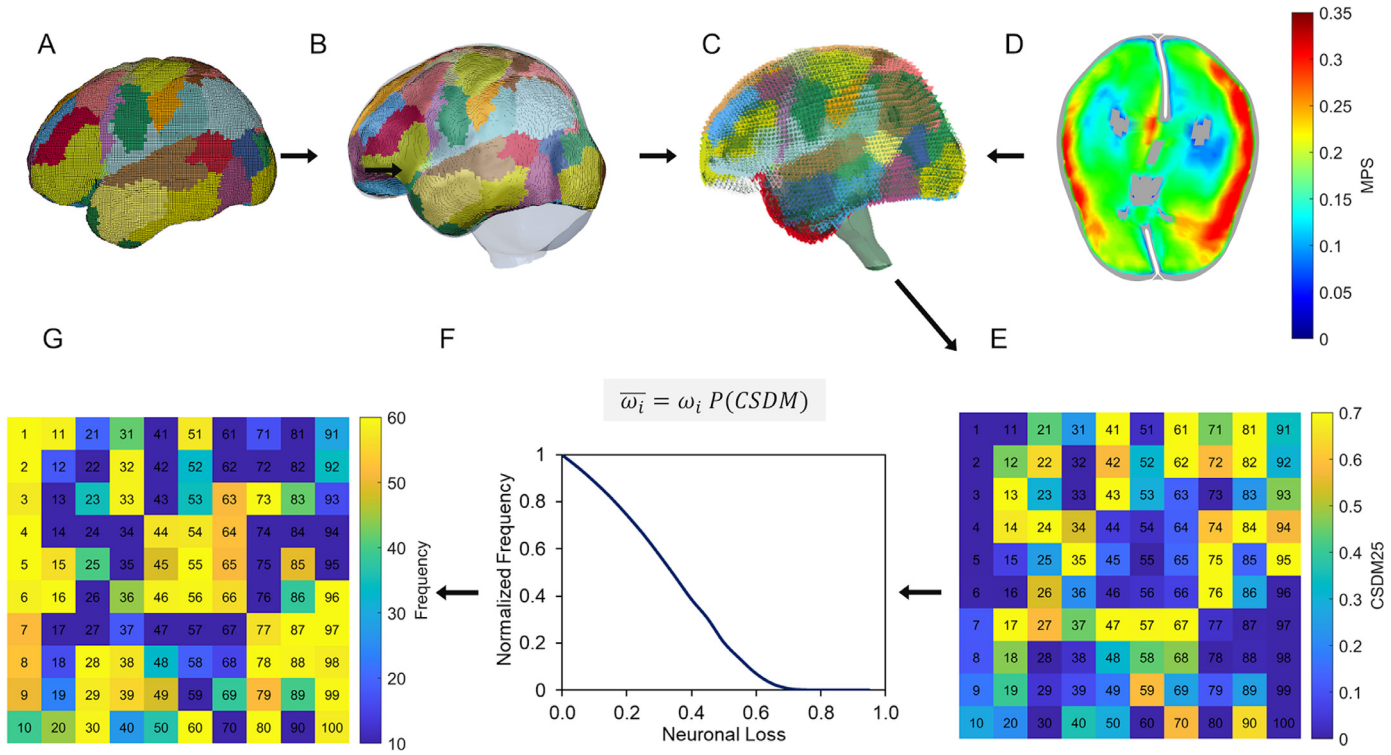

Fig. 3. Summary of the node-based method. (A) Schaefer parcellation atlas was converted into a voxel model in which each voxel in the MRI is converted to a single cubic hexahedral element; (B) The voxel model was then morphed to match with the FE model using a morphing technique described in (Wu et al., 2019a); (C) Solid elements in the FE model were segmented into different ROIs; (D) Maximum principal strain at a cross-section plane of the brain under a concussive impact (ID: 2754); (E) CSDM matrix for the given impact; (F) Correlation between CSDM (percentage of neuronal loss) and normalized frequency; (G) Decreased frequency for each oscillator (1–100) after the head impact.

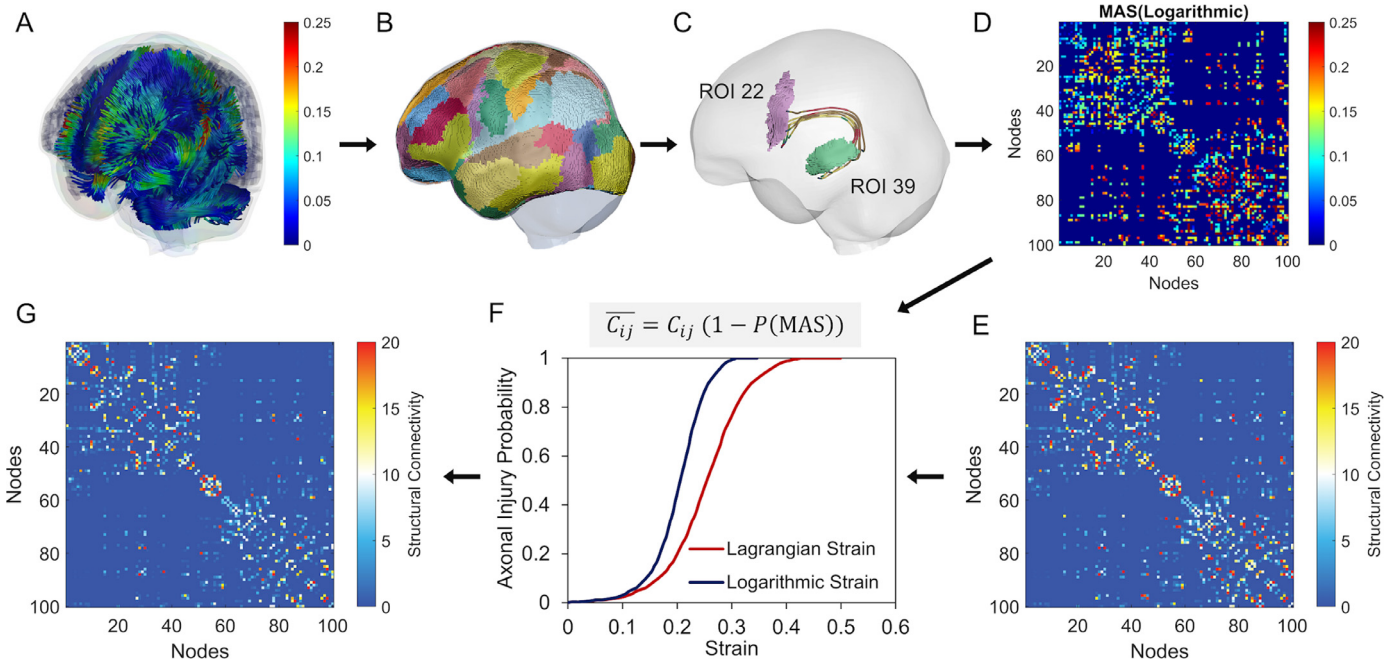

Fig. 4. Summary of the edge-based method. (A) Maximum axonal logarithmic strain of a concussive impact (ID: 2754); (B) Schaefer parcellation atlas was converted into a voxel model in which each voxel in the MRI is converted to a single cubic hexahedral element; the voxel model was then morphed to the FE model; (C) Axonal tracts in the FE model was segmented out by ROIs; (D) Maximum axonal logarithmic strain matrix for the given impact; (E) Healthy structural connectivity; (F) Alteration of the original edge value in SC based on the probability of injury for axonal tracts, and mechanical tolerance for axonal injury based on Lagrangian and Logarithmic strain (Bain and Meaney, 2000); (G) Injured structural connectivity.

Table 2
Summary of simulation and analysis. A series of simulations evaluated the dynamics and functional connectivity that occurred in a healthy subject, and this same subject when different injury models (node-based, edge-based, combined) were used. As a comparison, we also evaluated the changes when starting with a randomized network. Measure of both the dynamics and functional connectivity were compared to kinematic measures of the impact, and traditional tissue-based injury criterion.

Simulations	Evaluated Metrics					
	Neural dynamics	Topological measures of FC	Changes of FC	Topological measures of SC	Topological measures of SC	Head kinematics and strain measures
None	N/A					
Random	Meta, Sync	CPL_{FC}, GE_{FC},	GD_{FC},	N/A		ω_{max}, α_{max},
Node-based (CSDM25)		CC_{FC},	PC_{FC}			MPS95,
Node-based (CSDM15)		LE_{FC},				CSDM25
Edge-based		M_{FC}				
Combined (CSDM25)				CPL_{SC},	GD_{SC}, PC_{SC}	
Combined (CSDM15)				GE_{SC},		
				CC_{SC},		
				LE_{SC},		
				M_{SC}		

cortical parcellations based on a Poisson disk sampling (Messé, 2020). We randomized the connections in the network by reshuffling the existing edges in the network; doing so preserved the weight, degree, and strength distributions. We used this randomized network - which consisted of both the random parcellation and random network connections - to simulate healthy subject dynamics and to predict changes that occurred in our best performing injury model (node-based injury with a critical threshold of 15% (CSDM15)). The same parameter settings used in the real subject (108,020) for Kuramoto model and hemodynamic model were adopted for these simulations.

2.7. Data analysis

The different lesion methods and their combinations result in five types of simulations; the available injury metrics for each type, along with the simulation using a randomized network, are summarized in Table 2. Logistic regression analysis was used to evaluate the correlation between continuous metrics and binary injury data (injury vs. no injury). The receiver operating characteristic (ROC) curve was used to assess how well the metric discriminates individuals with or without injury. ROC curves are summarized in a single value: the area under the ROC curve (AUC). Delong statistical tests were used to determine whether one measure has a significantly different AUC than another measure (DeLong et al., 1988; Robin et al., 2011). The Akaike information criterion (AIC) was used to compare the goodness of fit and relative quality of statistical models (Akaike, 1974). The AIC is defined as

$$AIC = -2log\ (L)\ + 2V$$

Where L is the maximum likelihood for the candidate model, V is the number of independent variables (Note that $V = 1$ in this study).

3. Results

3.1. Kuramoto oscillator model parameters search

Our first step developed a modeling pipeline to accurately represent measures of functional connectivity in a human subject. To this end, the global coupling constant (K) and the mean time delay (τ) were optimized to match the simulated healthy FC with the empirical FC data. The simulated FC obtained at $K = 11.5$, and $\tau = 6\ ms$ showed the best agreement with the empirical FC measured from a subject with a structural connectivity matrix resembling the average connectivity across a population of 1065 subjects (Fig. 5A). The optimal simulated FC and empirical FC also had similar global efficiency (Fig. 5B). In this set of parameters, the oscillators are only moderately synchronized (Sync= 0.560) and in a metastable regime (Meta=0.127) (Fig. 5C and D).

3.2. TBI metrics evaluation

Using the extracted parameter sets ($K = 11.5$ and $\tau = 6\ ms$) from the parameter search, we simulated the disruption of brain networks using the node-based method, or the edge-based method, or the combined injury method. A visualization of simulated FCs for an injurious and a noninjurious impact using the edge-based method, compared with simulated FC of the healthy subject, is depicted in Fig. 6. Indicated by AUC and AIC (Fig. 7A–D), most topological measures of the SC (except for modularity) performed as good as (Fig. 7E, $p > 0.05$) the traditional measures (ω_{max}, AUC=0.85; α_{max}, AUC=0.90; MPS95, AUC=0.88; CSDM25, AUC=0.88) in predicting injury outcomes. The prediction performance of FC-related measures depended on lesion methods, but none of the measures outperformed the traditional measures. The best predictive models using FC-based approaches occurred when using either a node-based method (CSDM15), or a combination of injury to the gray matter nodes and white matter edges in the network (Combined CSDM15). Regardless of the specific injury methods, good correlations ($AUC > 0.75$, $AIC < 65$) occurred between injury outcomes and predictors, including local efficiency (LE_{FC}), clustering coefficient (CC_{FC}), and Pearson correlation (PC_{FC}) of FCs (Fig. 7B and D). However, the directions of these correlations are not always consistent across injury methods (Fig. 8). When using the node-based method, global efficiency (GE_{FC}), local efficiency (LE_{FC}), clustering coefficient (CC_{FC}) were positively correlated with injury risk, while these metrics were negatively correlated with injury risk when using the edge-based method.

The combined model, which included the effect of impact to both nodes and edges in the functional brain networks, produced more complex correlations to the presence or absence of concussive injury. As mentioned above, the node-based and edge-based injury had opposite effects on some measures of the FCs. Therefore, the prediction performance was sensitive to the thresholds used to determine neurodegeneration and mechanical tolerance for axonal injury. If the threshold for damage to the node oscillators was set at a higher value (CSDM25), the combined (CSDM25) method performed poorly in predicting injury compared to the separate (node-based or edge-based) methods. However, if the threshold for injury to the nodes was set at a lower value (CSDM15), the performance of the combined (CSDM15) method did not significantly (Fig. 7E) differ from the node-based model using the same threshold (CSDM15). When the CSDM threshold was set lower, the combined model performance is influenced more by the node-based change in frequency, instead of the edge-based reduction in structural connections.

When the atlas-based parcellation and image-based brain network were replaced by a randomized network (with preserved weight, degree, and strength distributions), several changes occurred. For unin-

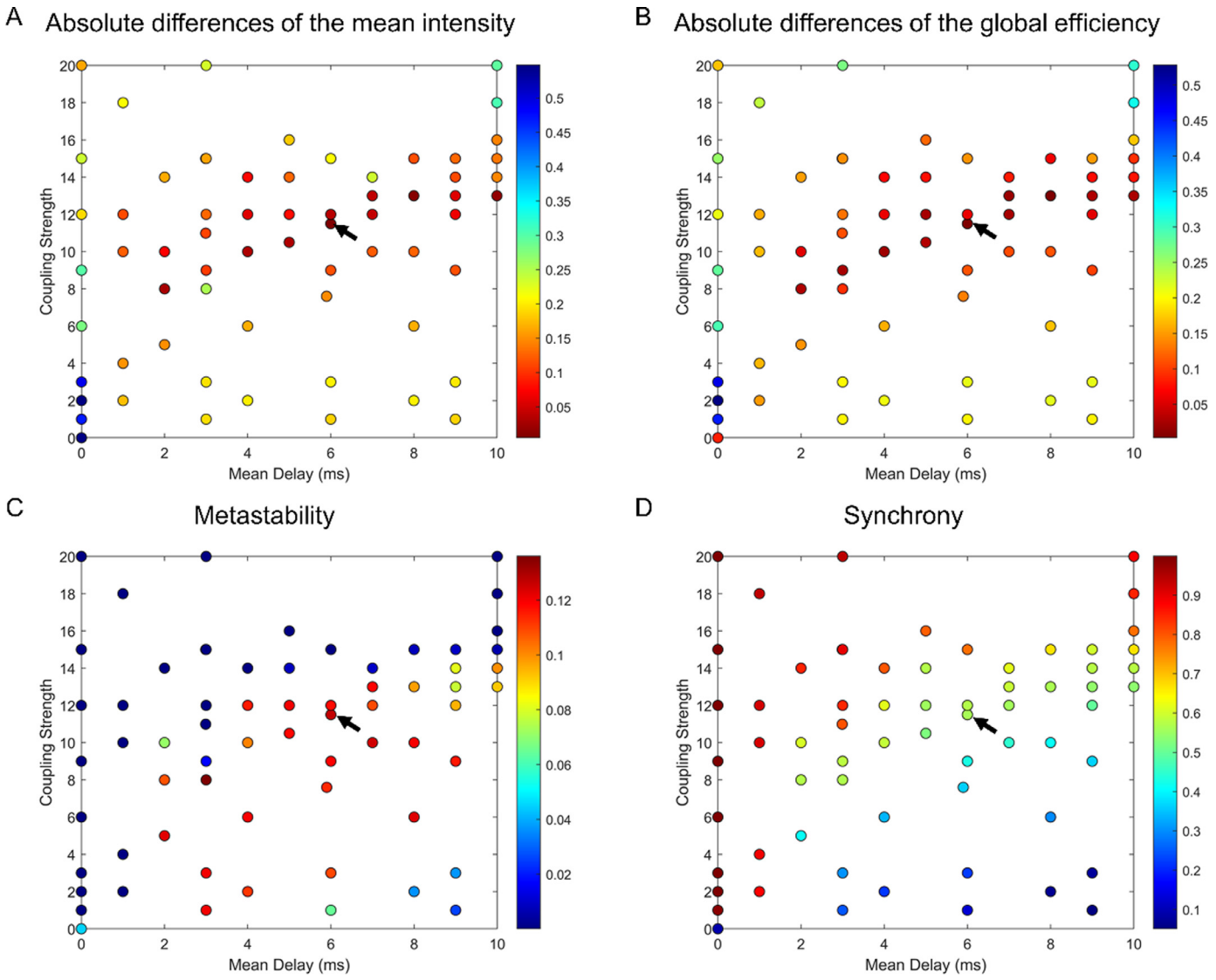

Fig. 5. Response across parameter space. (A) Absolute differences between the mean absolute values of the simulated and empirical FC matrices; warmer colors indicate a better fit between model and measured dynamics (B) Absolute differences between the global efficiency of the simulated and empirical FC; Arrows in (a) and (B) indicate optimal coupling strength and mean delay parameter combinations. (C) Global metastability and (D) global synchrony. With parameters showing the best fit between measured and predicted functional connectivity (arrows), the network showed modest synchrony and high metastability.

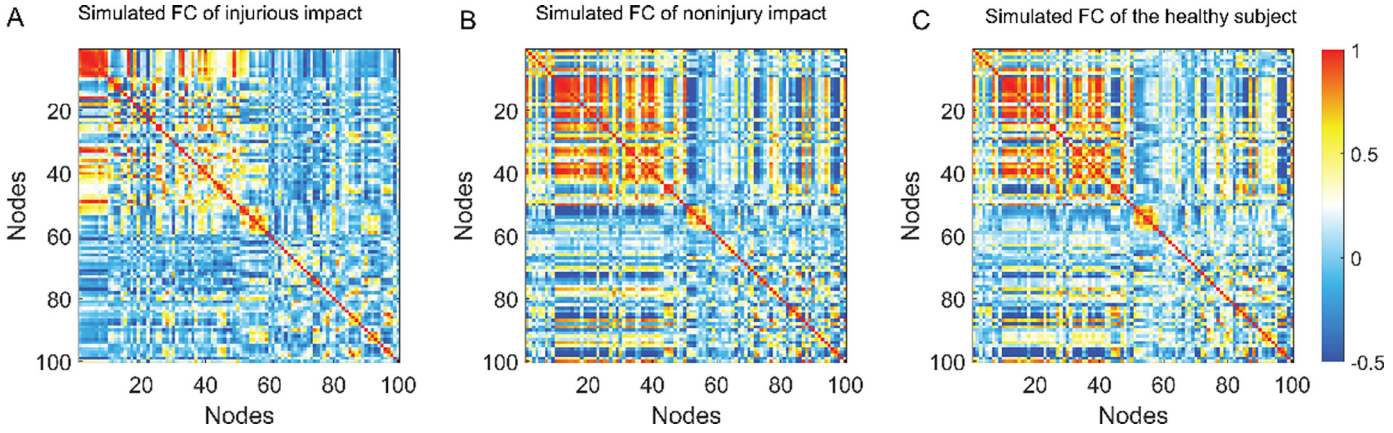

Fig. 6. Example of simulated FCs of injurious and noninjury impact, comparing with simulated FC of the healthy subject. (A) Simulated FC of injurious impact; (B) Simulated FC of noninjury impact; (C) Simulated FC of the healthy subject. The edge-based injury method was used for the shown examples.

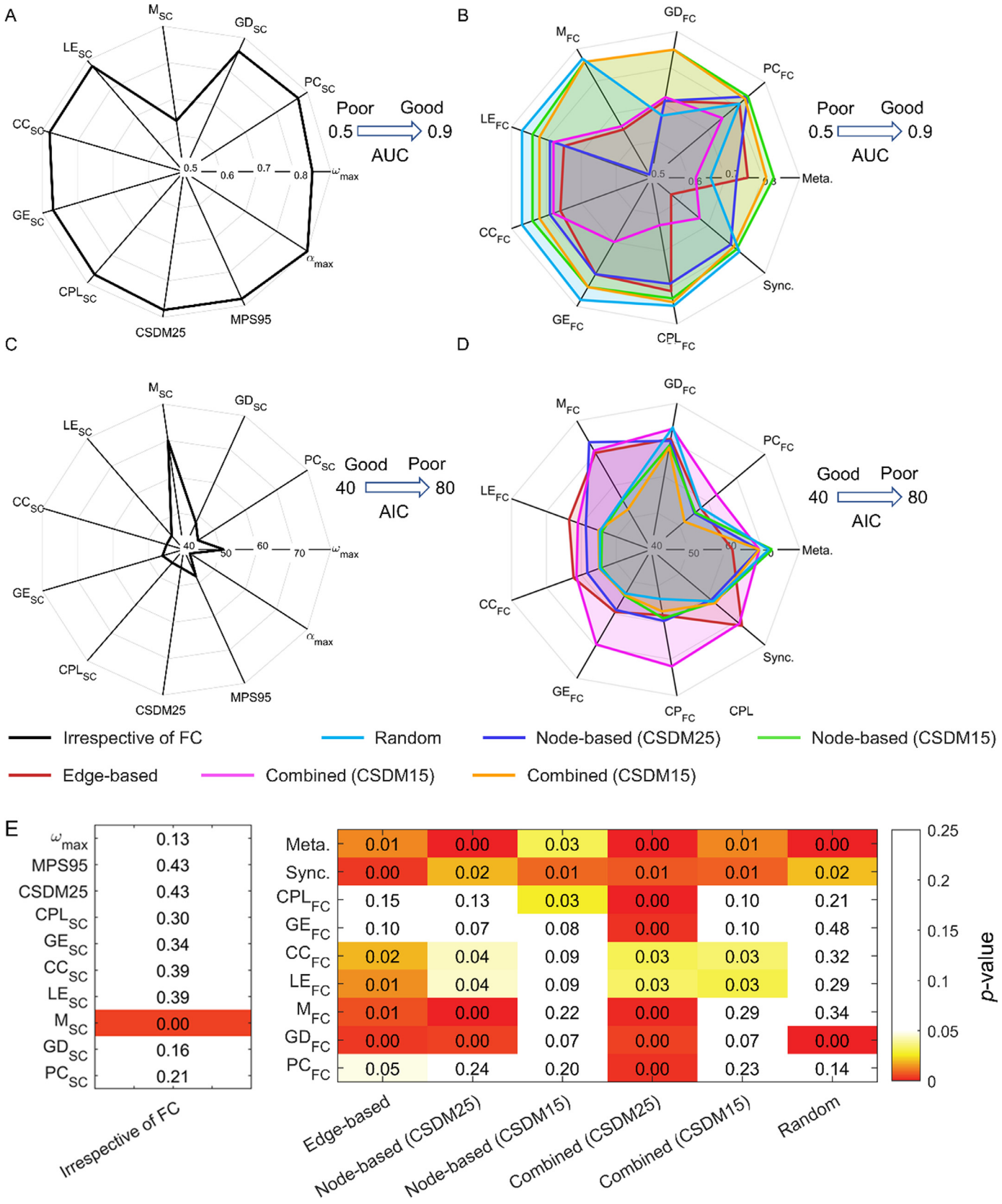

Fig. 7. Summary of performance. (A) AUC of metrics which are not related to FC; (B) AUC of FC-related metrics; (C) AIC of metrics which are not related to FC; (D) AIC of FC-related metrics; A higher AUC indicates better performance, and a lower AIC indicates a better fit; (E) Uncorrected p-values obtained with DeLong's test to determine whether one measure has a significantly different AUC than the measure of the highest AUC (α_{max}); Significant values were highlighted with color according to the 5% significant level.

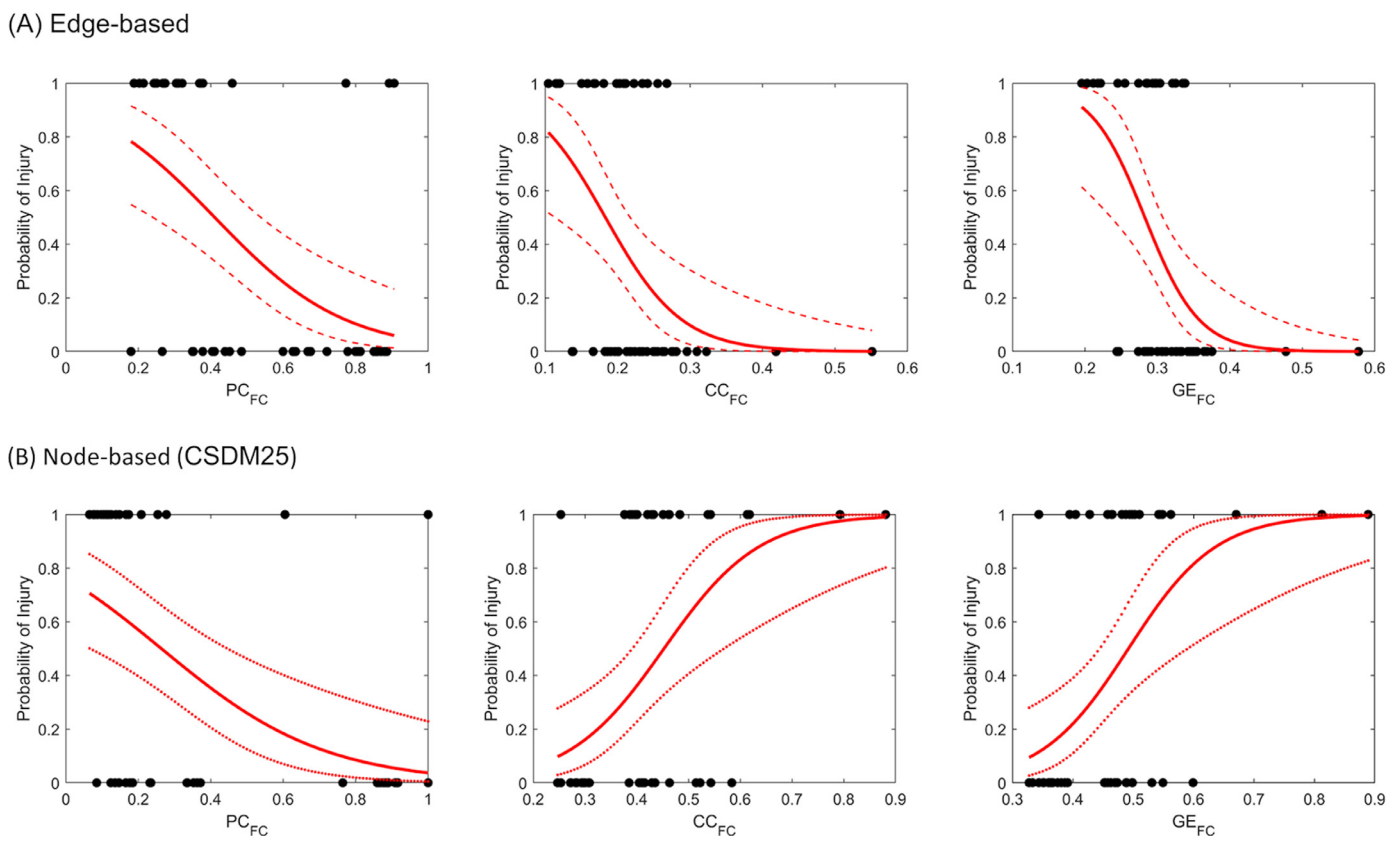

Fig. 8. Example of the logistic regression between injury metrics and injury outcomes. (A) Results based on edge-based injury method; (B) Results based on node-based (CSDM25) injury method. Note that clustering coefficient (CC_{FC}) and global efficiency (GE_{FC}) were negatively correlated with injury risk when using the edge-based method, and positively correlated with injury risk when using the node-based method.

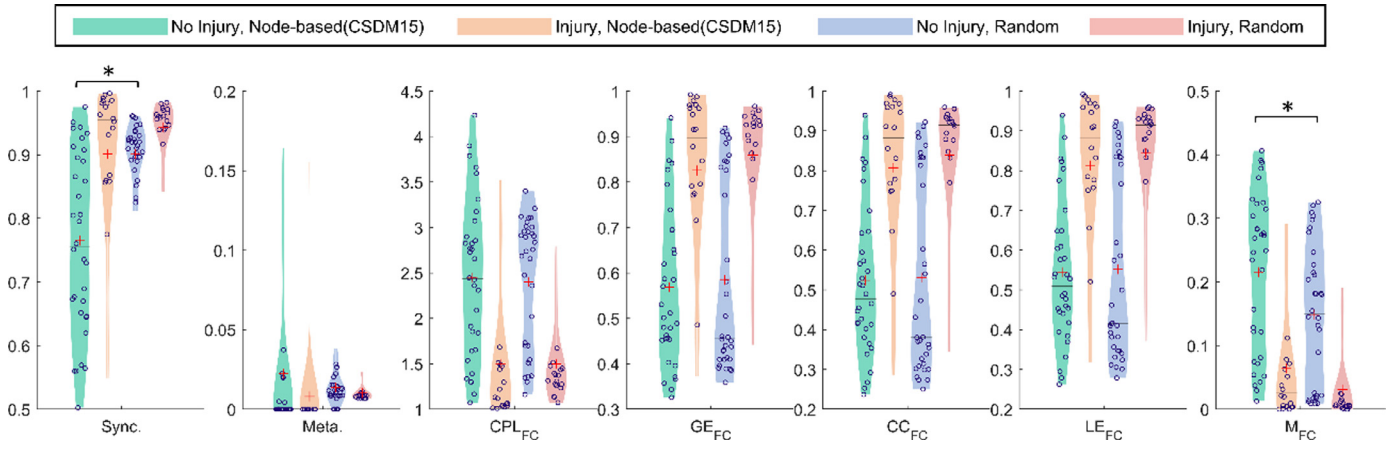

Fig. 9. Distributions of neurodynamic and topological metrics across different initial structural network conditions. Networks were either real or randomized and were uninjured or injured. Significant tests (*t*-test) were conducted between uninjured real network and uninjured random network, and between injured real network and injured random network, cases determined to be significantly different ($p<0.05$) were pointed out by the asterisk symbols.

jured networks, the randomization of the parcellations and the structural edge weights significantly changed modularity, but the changes were not reflected by the characteristic path length, global efficiency, local efficiency, and clustering coefficients (Fig. 9). Perhaps due to these changes in the network topology, randomization caused a significant increase in synchrony ($p<0.05$) and marginal difference in metastability (Fig. 9). As expected, injury caused significant changes in both structural and functional network measures, as the global topological measures and Pearson correlation of FCs were still correlated well ($AUC > 0.8$, $p > 0.05$) with injury outcomes using a node-based method (CSDM15). Not all measures, however, remained good predictors of injury, and the prediction performance of metastability and geodesic distances (GD_{FC}) degraded.

A second consideration was whether these results were substantially affected when a different brain architecture was used. To test the reliability of our observations, we used a different network architecture (ID:100,307) and a different set of parameters (Fig. A1, $K = 7.6$, and τ=5.9 ms), as shown in supplementary Section A3. These results confirmed that (i) FC-related measures worked as well as traditional metrics for predicting injury; (ii) among the FC-related measures, good cor-

relations occurred between injury outcomes and Pearson correlation (PC_{FC}) of FCs, and (iii) injury to a random network also led to significant changes in network function.

4. Discussion

An interdisciplinary computational model for predicting TBI was developed by coupling biomechanical models with neural dynamics and perfusion models. Although several studies (Alstott et al., 2009; Cabral et al., 2012; Honey and Sporns, 2008; van Dellen et al., 2013; Váša et al., 2015) studies how targeted changes to the connection network - e.g., removing the top 5% of nodes with highest connectivity - none of artificial lesioning approaches tried to mimic the actual degeneration patterns observed over time in neurological disease, or after acute injury. Our approach used a method to affect both the strength of connections across brain regions after an impact, as well as changes that could occur in nodal oscillators within a brain network after impact. Explicitly modeling how impacts could affect the initiation and transmission of information through brain networks led to a consistently good correlation with injury outcomes (AUC=0.75–0.84), indicating a potential predictive method for assessing outcome after impact. In comparison, intentionally randomizing the nodal organization and connections across nodal regions in the brain significantly affected the baseline neural dynamics, and affected the ability of using some metrics (such as metastability) to distinguish injured from uninjured networks. However, our different lesion methods had opposing effects between topological measures and injury outcomes, thereby making it difficult to determine the optimal scheme for predicting injury risk. Our work is the first study to integrate both impact biomechanics and neural dynamics models to understand how rapid head motions can lead to underlying structural and functional impairment to the brain.

Conceptually, we built upon several past studies that used models to link brain structure to functional connectivity across brain regions. Similar to our study, neurodynamic models in this form (Cabral et al., 2014; Fukushima and Sporns, 2018; Lee et al., 2017; Váša et al., 2015) were unable to reproduce empirical functional connectivity perfectly. The lack of a perfect match between our model and the measured data is not surprising, given the relative simplicity of the model. Although one might consider the model choice as one reason for this discrepancy, previous studies (Messé et al., 2014, 2015) demonstrated that the prediction accuracy of the Kuramoto model is comparable to that of other major computational neurodynamic models (e.g., neural mass model). Still, a clear pattern exists, which is sufficient to identify an area of parameter space where the model best approximates empirical data. The model optimally predicts empirical FC for a range of parameters where the oscillators exhibit relatively low synchrony and high metastability. This pattern corresponds to the same dynamical regime where the best agreement with BOLD (Fukushima and Sporns, 2018) or MEG (Cabral et al., 2014) functional connectivity was found in previous work.

Our results also explored how a random re-parcellation and rewiring affected the baseline levels of neurodynamics and functional connectivity, as well as the change which occurs after an impact. As expected, a completely randomized network significantly changed the baseline measures of neural activity and functional connectivity relative to the original network, although the changes were not well characterized by the global topological measures of functional network. On its own, these results suggest the network topology is critically coupled to neurodynamics and functional connectivity. Every impact we simulated led to a broad pattern of deformation throughout the entire brain; for this reason, injury also affected our randomized network in a similarly diffuse manner. Any impact generally caused reductions in nodal oscillator frequencies, causing subsequent increase in functional coupling, regardless of whether the network was organized or random. As impact intensity increases, the deformation throughout the brain increases in extent and magnitude (Wu et al., 2021) to cause a more progressive loss in oscillator frequencies and increase in synchrony and functional coupling. Together, these observations suggest that the network configuration is important to establish the baseline communication characteristics of a network, but the injury effect is sufficiently widespread throughout the network that any network, regardless of its configuration, will show clear changes after an impact.

When considering brain architecture, function, and impact conditions together, our results show that network-based analysis can provide predictors of injury outcome that are equal to traditional methods (kinematics-based metrics and strain measures) that do not consider any aspect of either brain organization or dynamics. Our closest correlations between traditional injury threshold measures and network-based predictions of injury occurred when we focused on changes related to the structural connectome after impact. In many cases, the performance of most global measures of the SC is as good as traditional metrics of rotational motions. This high correlation is expected because the changes to the structural connectome are tied closely to deformation occurring within the brain, which is influenced directly by the loading kinematics (Alshareef et al., 2020; Gabler et al., 2018; Wu et al., 2020). Certainly, the uncertainty in the loading impact conditions can affect the accuracy of the injury predictions, as recognized before (Anderson et al., 2020), but this factor would affect both kinematics and deformation-based predictors. One additional consideration for structural connectome-based metrics would be the difference in the individual brain anatomy and architecture, each of which could change the accuracy in predicting concussion risk across a population. To address this concern, though, we confirmed that the general findings were observed when using a different network architecture and a different set of parameters in the Kuramoto model.

The reliability of inferences drawn from this model also depends on the biofidelity and the accuracy of the mesoscopic fiber architecture of the FE brain model. The FE brain model demonstrated good biofidelity compared to the other state-of-the-art models when simulating the latest human brain deformation data (Wu et al., 2019a). The mesoscopic fiber architecture modeled in the FE model was extracted from the population-averaged tractography. However, due to the high computational cost, the resulting tractography included in the FE model only has 3446 fiber tracts, which are greatly underrepresented compared to the tracts (1000,000) reconstructed to calculate the structural connectome. This discrepancy and the individual variability of the tractography in the population would introduce error into the model especially when using the edge-based method.

Perhaps the most challenging part of the analysis was to examine the potential correlations that could occur between the functional network architecture and outcome (concussion/no concussion) after impact. Expecting a clear distinction between injured and uninjured architectures may be too ambitious, as clinical data suggested brain networks of injured and healthy groups showed no statistically significant differences in the *global* metrics (e.g., density, global efficiency, modularity, clustering coefficient) of functional networks in the (sub)acute phase (within three months) after TBI (Virji-Babul et al., 2014). Likewise, demonstrating a clear match between our predicted changes in functional architecture and the clinical evidence of connectivity changes would be difficult, as empirical studies measured connectivity days post-injury and the recovery of the connectivity could mask some of the immediate changes occurring right after impact (Dall'Acqua et al., 2017). Moreover, these topological measures were initially developed to describe unweighted (or binary), undirected networks (e.g., social networks), and the extension of these metrics to weighted, directed networks is not always straightforward. To characterize FC with negative weights, we removed negative connections from the networks prior to analysis. A possible alternative procedure in brain graph analysis is to consider the absolute value of the resulting correlation coefficient regardless of its sign (Achard et al., 2006), which could also present difficulties in terms of neurophysiological interpretation (Buckner, 2010). However, a preliminary analysis of the injury prediction performance shows that the general findings are relatively consistent when we use different procedures

for calculating topological measures of FCs (see Supplemental A3). Finally, our analysis used global measures of network architecture, which is distinct from most empirical studies which focused on differences of local measures between healthy and injured groups (Borich et al., 2015; Churchill et al., 2018; Mayer et al., 2011; Meier et al., 2017; Murdaugh et al., 2018; Orr et al., 2016; Plourde et al., 2020; Virji-Babul et al., 2014). Future work could consider whether better correlations would occur with local network measures. For example, head rotation direction was found to significantly affect the severity and outcome of injury (Cullen et al., 2016; Gennarelli et al., 1987; Ibrahim et al., 2010). It is possible that the directional dependence of TBI outcome may be due to the preferential changes in these local networks.

Our results clearly demonstrate a delicate balance among the effects of injury to both gray and white matter simultaneously. Removing or reducing the connectivity of strongly connected oscillating nodes in a network would clearly impair the ability to synchronize the network, as well as the efficiency of transferring information through the network. Both of these network features are considered important for cognitive processing (Aerts et al., 2016). However, the real-world impact conditions we studied do not preferentially affect edges from only strongly connected nodes. Rather, edges throughout the network are affected and this distributive effect is most noticeable with a dramatic reduction in the efficiency of the network. In comparison, it is well known that the deformations (strain) within the brain are high along the periphery, near partitioning membranes, and in regions where separate brain areas can shift quickly during impact (e.g., corpus callosum) (Alshareef et al., 2020). For this reason, it is likely that any impact would significantly affect the broad network of gray matter nodes in our network and lead to a more heterogeneous mix of oscillator frequencies. As a result, the efficiency of the functional network tends to increase when considering the effect of only gray matter injury, in contrast to a reduction in efficiency when only considering damage to the network edges.

Clearly this balance between synchronizing and efficiently passing information through a network will be affected by the thresholds used in the different lesion methods. For example, increasing the threshold for gray matter changes in the network dynamics will bias the prediction towards the edge lesion methods, and vice versa. Our most accurate prediction of injury occurred when gray and white matter damage occurred at approximately the same mechanical threshold (~15%). Therefore, our results imply the mechanical tolerance of different parts of the brain is similar. If proven correct, this finding would change our perspective on how immediate neurological impairments occur following concussion. Historically, mild traumatic brain injury was viewed as a diffuse injury, where the microscopic damage appearing throughout the white matter was considered the primary neuropathological component of the injury (Johnson et al., 2013; Smith and Meaney, 2000). Based on this observation, much of the past work considering the tolerance of the brain to impact focused on how the extent of white matter damage would contribute towards injury risk (Hajiaghamemar et al., 2020; Sahoo et al., 2016; Wu et al., 2021). Certainly, the long-lasting impairments after mild TBI may still link most critically to permanent changes to the white matter (Johnson et al., 2013; Shenton et al., 2012; Smith and Meaney, 2000), as neuronal degeneration is not considered a primary feature of either the acute or chronic phase of mTBI (Gardner and Yaffe, 2015). However, our findings indicate that changes to the gray matter (nodes) and white matter (edges) are both important for determining the network organization immediately after impact and are therefore both critical for rebuilding and recovering network function after impact. Recovering oscillating nodes for promoting network recovery is conceptually consistent with clinical tools to stimulate different cortical areas and treat neurological disorders, some of which show promise for treating TBI patients (Bonnì et al., 2013; Kundu et al., 2018; Zaninotto et al., 2019). A key step in this network reconstruction process would be considering how the stimulation re-routes existing pathways in the brain to counteract permanent changes to the network edges that could appear after mild TBI (Castellanos et al., 2011; Kantak et al., 2012; Kuceyeski et al., 2019). In this manner, the accurate prediction of the network structure after an impact would be equally important to determine safe and unsafe impact conditions, as well as potential restorative strategies for cognitive function.

This work contributes to bridging the missing link between the neural network and injury biomechanics. We showed how rapid head motions could lead to the disruption of structural and functional networks at a causal mechanistic level. This work provides a foundation for and highlights the possibility of applying network analysis in clinical practice for TBI. Since the individual information about the brain anatomy and network architecture of the involved football players is not available, this study used one generic FE model and one generic network architecture. Going forward, further work exploring a variety of brain morphology and network architectures could shed light on the susceptibility to concussion among the population under different impact conditions and improve the design of subject-specific head protection equipment. Because of its capability of considering different anatomical factors from both biomechanical and neurodynamic perspectives, the framework developed in this study is a crucial tool to facilitate future multi-dimensional exploration.

Data and code availability

The diffusion MRI and functional MRI data are available through Human Connectome Project (https://www.humanconnectome.org/study/hcp-young-adult). The parcellation atlas is publicly available on Github (https://github.com/ThomasYeoLab/CBIG/tree/master/stable_projects/brain_parcellation/Schaefer2018_LocalGlobal). The football impacts data is available through Biokinetics and Associates Ltd.

Declaration of Competing Interest

No competing financial interests exist.

Credit authorship contribution statement

Taotao Wu: Conceptualization, Methodology, Formal analysis, Investigation, Writing – original draft, Writing – review & editing. **Jared A Rifkin:** Formal analysis, Visualization, Writing – review & editing. **Adam Rayfield:** Formal analysis, Validation, Writing – review & editing. **Matthew B. Panzer:** Methodology, Writing – review & editing. **David F. Meaney:** Conceptualization, Formal analysis, Writing – review & editing, Supervision, Funding acquisition.

Acknowledgments

This work was funded by the Paul G. Allen Foundation. Neuroimaging data were provided by the Human Connectome Project, WU-Minn Consortium (Principal Investigators: David Van Essen and Kamil Ugurbil; 1U54MH091657) funded by the 16 NIH Institutes and Centers that support the NIH Blueprint for Neuroscience Research; and by the McDonnell Center for Systems Neuroscience at Washington University.

Supplementary materials

Supplementary material associated with this article can be found, in the online version, at doi:10.1016/j.neuroimage.2022.119002.

References

Achard, S., Salvador, R., Whitcher, B., Suckling, J., Bullmore, E., 2006. A resilient, low-frequency, small-world human brain functional network with highly connected association cortical hubs. J. Neurosci. 26 (1), 63–72.

Aerts, H., Fias, W., Caeyenberghs, K., Marinazzo, D., 2016. Brain networks under attack: robustness properties and the impact of lesions. Brain 139 (12), 3063–3083.

Akaike, H., 1974. A new look at the statistical model identification. In: Selected Papers of Hirotugu Akaike. Springer, pp. 215–222.

Alshareef, A., Giudice, J.S., Forman, J., Shedd, D.F., Reynier, K.A., Wu, T., Sochor, S., Sochor, M.R., Salzar, R.S., Panzer, M.B., 2020. Biomechanics of the human brain during dynamic rotation of the head. J. Neurotrauma 37 (13), 1546–1555.
Alshareef, A., Wu, T., Giudice, J.S., Panzer, M.B., 2021. Toward subject-specific evaluation: methods of evaluating finite element brain models using experimental high-rate rotational brain motion. Biomech. Model. Mechanobiol. 20 (6), 2301–2317.
Alstott, J., Breakspear, M., Hagmann, P., Cammoun, L., Sporns, O., 2009. Modeling the impact of lesions in the human brain. PLoS Comput. Biol. 5 (6), e1000408.
Anderson, E.D., Giudice, J.S., Wu, T., Panzer, M.B., Meaney, D.F., 2020. Predicting concussion outcome by integrating finite element modeling and network analysis. Front. Bioeng. Biotechnol. 8, 309.
Bain, A.C., Meaney, D.F., 2000. Tissue-level thresholds for axonal damage in an experimental model of central nervous system white matter injury. J. Biomech. Eng. 122 (6), 615–622.
Bonnì, S., Mastropasqua, C., Bozzali, M., Caltagirone, C., Koch, G., 2013. Theta burst stimulation improves visuo-spatial attention in a patient with traumatic brain injury. Neurol. Sci. 34 (11), 2053–2056.
Borich, M., Babul, A.N., Yuan, P.H., Boyd, L., Virji-Babul, N., 2015. Alterations in resting-state brain networks in concussed adolescent athletes. J. Neurotrauma 32 (4), 265–271.
Buckner, R.L., 2010. Human functional connectivity: new tools, unresolved questions. Proc. Natl. Acad. Sci. 107 (24), 10769–10770.
Cabral, J., Hugues, E., Kringelbach, M.L., Deco, G., 2012. Modeling the outcome of structural disconnection on resting-state functional connectivity. Neuroimage 62 (3), 1342–1353.
Cabral, J., Luckhoo, H., Woolrich, M., Joensson, M., Mohseni, H., Baker, A., Kringelbach, M.L., Deco, G., 2014. Exploring mechanisms of spontaneous functional connectivity in MEG: how delayed network interactions lead to structured amplitude envelopes of band-pass filtered oscillations. Neuroimage 90, 423–435.
Castellanos, N.P., Leyva, I., Buldú, J.M., Bajo, R., Paúl, N., Cuesta, P., Ordóñez, V.E., Pascua, C.L., Boccaletti, S., Maestú, F., 2011. Principles of recovery from traumatic brain injury: reorganization of functional networks. Neuroimage 55 (3), 1189–1199.
Churchill, N.W., Hutchison, M.G., Graham, S.J., Schweizer, T.A., 2018. Connectomic markers of symptom severity in sport-related concussion: whole-brain analysis of resting-state fMRI. Neuroimage Clin. 18, 518–526.
Cullen, D.K., Harris, J.P., Browne, K.D., Wolf, J.A., Duda, J.E., Meaney, D.F., Margulies, S.S., Smith, D.H., 2016. A porcine model of traumatic brain injury via head rotational acceleration. In: Injury Models of the Central Nervous System. Springer, pp. 289–324.
Dall'Acqua, P., Johannes, S., Mica, L., Simmen, H.P., Glaab, R., Fandino, J., Schwendinger, M., Meier, C., Ulbrich, E.J., Müller, A., 2017. Functional and structural network recovery after mild traumatic brain injury: a 1-year longitudinal study. Front. Hum. Neurosci. 11, 280.
DeLong, E.R., DeLong, D.M., Clarke-Pearson, D.L., 1988. Comparing the areas under two or more correlated receiver operating characteristic curves: a nonparametric approach. Biometrics 44 (3), 837–845.
Fries, P., 2005. A mechanism for cognitive dynamics: neuronal communication through neuronal coherence. Trends Cogn. Sci. (Regul. Ed.) 9 (10), 474–480.
Friston, K.J., Mechelli, A., Turner, R., Price, C.J., 2000. Nonlinear responses in fMRI: the Balloon model, Volterra kernels, and other hemodynamics. Neuroimage 12 (4), 466–477.
Fukushima, M., Sporns, O., 2018. Comparison of fluctuations in global network topology of modeled and empirical brain functional connectivity. PLoS Comput. Biol. 14 (9), e1006497.
Gabler, L.F., Crandall, J.R., Panzer, M.B., 2018. Development of a metric for predicting brain strain responses using head kinematics. Ann. Biomed. Eng. 46 (7), 972–985.
Gabler, L.F., Crandall, J.R., Panzer, M.B., 2019. Development of a second-order system for rapid estimation of maximum brain strain. Ann. Biomed. Eng. 47 (9), 1971–1981.
Gabrieli, D., Schumm, S.N., Vigilante, N.F., Parvesse, B., Meaney, D.F., 2020. Neurodegeneration exposes firing rate dependent effects on oscillation dynamics in computational neural networks. PLoS One 15 (9), e0234749.
Gardner, R.C., Yaffe, K., 2015. Epidemiology of mild traumatic brain injury and neurodegenerative disease. Mol. Cell. Neurosci. 66, 75–80.
Garimella, H.T., Kraft, R.H., 2017. Modeling the mechanics of axonal fiber tracts using the embedded finite element method. Int. J. Numer. Method Biomed. Eng. 33 (5), e2823.
Gennarelli, T.A., Thibault, L.E., Tomei, G., Wiser, R., Graham, D., Adams, J., 1987. Directional Dependence of Axonal Brain Injury Due to Centroidal and Non-Centroidal Acceleration. SAE Technical Paper.
Giordano, C., Kleiven, S., 2014. Evaluation of Axonal Strain As a Predictor For Mild Traumatic Brain Injuries Using Finite Element Modeling. SAE Technical Paper.
Giudice, J.S., Zeng, W., Wu, T., Alshareef, A., Shedd, D.F., Panzer, M.B., 2019. An analytical review of the numerical methods used for finite element modeling of traumatic brain injury. Ann. Biomed. Eng. 47 (9), 1855–1872.
Glasser, M.F., Sotiropoulos, S.N., Wilson, J.A., Coalson, T.S., Fischl, B., Andersson, J.L., Xu, J., Jbabdi, S., Webster, M., Polimeni, J.R., 2013. The minimal preprocessing pipelines for the human connectome project. Neuroimage 80, 105–124.
Hajiaghamemar, M., Wu, T., Panzer, M.B., Margulies, S.S., 2020. Embedded axonal fiber tracts improve finite element model predictions of traumatic brain injury. Biomech. Model. Mechanobiol. 19 (3), 1109–1130.
Hansen, K.R., DeWalt, G.J., Mohammed, A.I., Tseng, H., Abdulkerim, M.E., Bensussen, S., Saligrama, V., Nazer, B., Eldred, W.D., Han, X., 2018. Mild blast injury produces acute changes in basal intracellular calcium levels and activity patterns in mouse hippocampal neurons. J. Neurotrauma 35 (13), 1523–1536.
Hardy, W.N., Mason, M.J., Foster, C.D., Shah, C.S., Kopacz, J.M., Yang, K.H., King, A.I., Bishop, J., Bey, M., Anderst, W., Tashman, S., 2007. A study of the response of the human cadaver head to impact. Stapp Car Crash J. 51, 17–80 PubMed.
Honey, C.J., Sporns, O., 2008. Dynamical consequences of lesions in cortical networks. Hum. Brain Mapp. 29 (7), 802–809.
Ibrahim, N.G., Ralston, J., Smith, C., Margulies, S.S., 2010. Physiological and pathological responses to head rotations in toddler piglets. J. Neurotrauma 27 (6), 1021–1035.
Johnson, V.E., Stewart, W., Smith, D.H., 2013. Axonal pathology in traumatic brain injury. Exp. Neurol. 246, 35–43.
Kantak, S.S., Stinear, J.W., Buch, E.R., Cohen, L.G., 2012. Rewiring the brain: potential role of the premotor cortex in motor control, learning, and recovery of function following brain injury. Neurorehabil. Neural Repair 26 (3), 282–292.
Kraft, R.H., Mckee, P.J., Dagro, A.M., Grafton, S.T., 2012. Combining the finite element method with structural connectome-based analysis for modeling neurotrauma: connectome neurotrauma mechanics. PLoS Comput. Biol. 8 (8), e1002619.
Kuceyeski, A.F., Jamison, K.W., Owen, J.P., Raj, A., Mukherjee, P., 2019. Longitudinal increases in structural connectome segregation and functional connectome integration are associated with better recovery after mild TBI. Hum. Brain Mapp. 40 (15), 4441–4456.
Kundu, B., Brock, A.A., Englot, D.J., Butson, C.R., Rolston, J.D., 2018. Deep brain stimulation for the treatment of disorders of consciousness and cognition in traumatic brain injury patients: a review. Neurosurg. Focus 45 (2), E14.
Kuramoto, Y., 1984. Chemical turbulence. In: Chemical Oscillations, Waves, and Turbulence. Springer, pp. 111–140.
Latora, V., Marchiori, M., 2001. Efficient behavior of small-world networks. Phys. Rev. Lett. 87 (19), 198701.
Lee, W.H., Bullmore, E., Frangou, S., 2017. Quantitative evaluation of simulated functional brain networks in graph theoretical analysis. Neuroimage 146, 724–733.
Mao, H., Jin, X., Zhang, L., Yang, K.H., Igarashi, T., Noble-Haeusslein, L.J., King, A.I., 2010. Finite element analysis of controlled cortical impact-induced cell loss. J. Neurotrauma 27 (5), 877–888.
Mayer, A.R., Mannell, M.V., Ling, J., Gasparovic, C., Yeo, R.A., 2011. Functional connectivity in mild traumatic brain injury. Hum. Brain Mapp. 32 (11), 1825–1835.
Meaney, D.F., Morrison, B., Dale Bass, C., 2014. The mechanics of traumatic brain injury: a review of what we know and what we need to know for reducing its societal burden. J. Biomech. Eng. 136 (2), 021008.
Meier, T.B., Bellgowan, P.S., Mayer, A.R., 2017. Longitudinal assessment of local and global functional connectivity following sports-related concussion. Brain Imaging Behav. 11 (1), 129–140.
Messé, A., 2020. Parcellation influence on the connectivity-based structure–function relationship in the human brain. Hum. Brain Mapp. 41 (5), 1167–1180.
Messé, A., Rudrauf, D., Benali, H., Marrelec, G., 2014. Relating structure and function in the human brain: relative contributions of anatomy, stationary dynamics, and non-stationarities. PLoS Comput. Biol. 10 (3), e1003530.
Messé, A., Rudrauf, D., Giron, A., Marrelec, G., 2015. Predicting functional connectivity from structural connectivity via computational models using MRI: an extensive comparison study. Neuroimage 111, 65–75.
Mott, R.E., von Reyn, C.R., Firestein, B.L., Meaney, D.F., 2021. Regional neurodegeneration *in vitro*: the protective role of neural activity. Front. Comput. Neurosci. 15, 20.
Murdaugh, D.L., King, T.Z., Sun, B., Jones, R.A., Ono, K.E., Reisner, A., Burns, T.G., 2018. Longitudinal changes in resting state connectivity and white matter integrity in adolescents with sports-related Concussion–Erratum. J. Int. Neuropsychol. Soc. 24 (8), 890 –890.
Newman, M.E., 2006. Finding community structure in networks using the eigenvectors of matrices. Phys. Rev. E 74 (3), 036104.
Nguyen, T., Al-Juboori, M.H., Walerstein, J., Xiong, W., Jin, X., 2021. Impaired glutamate receptor function underlies early activity loss of ipsilesional motor cortex after closed-head mild traumatic brain injury. J. Neurotrauma 38 (14), 2018–2029.
Orr, C.A., Albaugh, M.D., Watts, R., Garavan, H., Andrews, T., Nickerson, J.P., Gonyea, J., Hipko, S., Zweber, C., Logan, K., 2016. Neuroimaging biomarkers of a history of concussion observed in asymptomatic young athletes. J. Neurotrauma 33 (9), 803–810.
Pellman, E.J., Viano, D.C., Tucker, A.M., Casson, I.R., Waeckerle, J.F., 2003. Concussion in professional football: reconstruction of game impacts and injuries. Neurosurgery 53 (4), 799–814.
Peterson, A.B., Xu, L., Daugherty, J., & Breiding, M.J. (2019). Surveillance report of traumatic brain injury-related emergency department visits, hospitalizations, and deaths, United States, 2014, Centers for Disease Control and Prevention, U.S. Department of Health and Human Services, Atlanta, GA
Plourde, V., Rohr, C.S., Virani, S., Bray, S., Yeates, K.O., Brooks, B.L., 2020. Default Mode Network Functional Connectivity After Multiple Concussions in Children and Adolescents. Oxford University Press.
Robin, X., Turck, N., Hainard, A., Tiberti, N., Lisacek, F., Sanchez, J.-C., Müller, M., 2011. PROC: an open-source package for R and S+ to analyze and compare ROC curves. BMC Bioinform. 12 (1), 1–8.
Rogers, E.A., Gross, G.W., 2019. Simultaneous electrophysiological and morphological assessment of functional damage to neural networks *in vitro* after 30–300 g impacts. Sci. Rep. 9 (1), 1–16.
Rubinov, M., Sporns, O., 2010. Complex network measures of brain connectivity: uses and interpretations. Neuroimage 52 (3), 1059–1069.
Sahoo, D., Deck, C., Willinger, R., 2016. Brain injury tolerance limit based on computation of axonal strain. Accid. Anal. Prev. 92, 53–70.
Sanchez, E.J., Gabler, L.F., Good, A.B., Funk, J.R., Crandall, J.R., Panzer, M.B., 2019. A reanalysis of football impact reconstructions for head kinematics and finite element modeling. Clin. Biomech. 64, 82–89.
Schaefer, A., Kong, R., Gordon, E.M., Laumann, T.O., Zuo, X.N., Holmes, A.J., Eickhoff, S.B., Yeo, B.T., 2018. Local-global parcellation of the human cerebral cortex from intrinsic functional connectivity MRI. Cereb. Cortex 28 (9), 3095–3114.
Shampine, L.F., Thompson, S., 2001. Solving ddes in matlab. Appl. Numer. Math. 37 (4), 441–458.

Shenton, M.E., Hamoda, H.M., Schneiderman, J.S., Bouix, S., Pasternak, O., Rathi, Y., Vu, M.-.A., Purohit, M.P., Helmer, K., Koerte, I., 2012. A review of magnetic resonance imaging and diffusion tensor imaging findings in mild traumatic brain injury. Brain Imaging Behav. 6 (2), 137–192.

Smith, D.H., Meaney, D.F., 2000. Axonal damage in traumatic brain injury. Neuroscientist 6 (6), 483–495.

van Dellen, E., Hillebrand, A., Douw, L., Heimans, J.J., Reijneveld, J.C., Stam, C.J., 2013. Local polymorphic delta activity in cortical lesions causes global decreases in functional connectivity. Neuroimage 83, 524–532.

Váša, F., Shanahan, M., Hellyer, P.J., Scott, G., Cabral, J., Leech, R., 2015. Effects of lesions on synchrony and metastability in cortical networks. Neuroimage 118, 456–467.

Venkatesh, M., Jaja, J., Pessoa, L., 2020. Comparing functional connectivity matrices: a geometry-aware approach applied to participant identification. Neuroimage 207, 116398.

Virji-Babul, N., Hilderman, C.G., Makan, N., Liu, A., Smith-Forrester, J., Franks, C., Wang, Z.J., 2014. Changes in functional brain networks following sports-related concussion in adolescents. J. Neurotrauma 31 (23), 1914–1919.

Wang, Y., Ghumare, E., Vandenberghe, R., Dupont, P., 2017. Comparison of different generalizations of clustering coefficient and local efficiency for weighted undirected graphs. Neural Comput. 29 (2), 313–331.

Watts, D.J., Strogatz, S.H., 1998. Collective dynamics of 'small-world'networks. Nature 393 (6684), 440.

Waxman, S.G., 2006. Axonal conduction and injury in multiple sclerosis: the role of sodium channels. Nat. Rev. Neurosci. 7 (12), 932–941.

Wu, S., Zhao, W., Rowson, B., Rowson, S., Ji, S., 2019a. A network-based response feature matrix as a brain injury metric. Biomech. Model. Mechanobiol. 19 (3), 927–942.

Wu, T., Alshareef, A., Giudice, J.S., Panzer, M.B., 2019b. Explicit modeling of white matter axonal fiber tracts in a finite element brain model. Ann. Biomed. Eng. 1–15. doi:10.1007/s10439-019-02239-8.

Wu, T., Antona-Makoshi, J., Alshareef, A., Giudice, J.S., Panzer, M.B., 2020. Investigation of cross-species scaling methods for traumatic brain injury using finite element analysis. J. Neurotrauma 37 (2), 410–422.

Wu, T., Hajiaghamemar, M., Giudice, J.S., Alshareef, A., Margulies, S.S., Panzer, M.B., 2021. Evaluation of tissue-level brain injury metrics using species-specific simulations. J. Neurotrauma 38 (13), 1879–1888.

Yeh, F.C., Panesar, S., Fernandes, D., Meola, A., Yoshino, M., Fernandez-Miranda, J.C., Vettel, J.M., Verstynen, T., 2018. Population-averaged atlas of the macroscale human structural connectome and its network topology. Neuroimage 178, 57–68.

Yeh, F.C., Tseng, W.Y.I., 2011. NTU-90: a high angular resolution brain atlas constructed by q-space diffeomorphic reconstruction. Neuroimage 58 (1), 91–99.

Yeung, M.S., Strogatz, S.H., 1999. Time delay in the Kuramoto model of coupled oscillators. Phys. Rev. Lett. 82 (3), 648.

Zaninotto, A.L., El-Hagrassy, M.M., Green, J.R., Babo, M., Paglioni, V.M., Benute, G.G., Paiva, W.S., 2019. Transcranial direct current stimulation (tDCS) effects on traumatic brain injury (TBI) recovery: a systematic review. Dement. Neuropsychol. 13 (2), 172–179.